IET Electric Power Applications

Research Article

IET Journals
The Institution of Engineering and Technology

Application of an improved discretisation method for the rotor-bearing assembly in the radiated noise analysis using Riccati transfer matrix method

ISSN 1751-8660
Received on 19th February 2017
Accepted on 6th April 2017
doi: 10.1049/iet-epa.2017.0107
www.ietdl.org

Chao Feng ✉, *Xiaochuan Ma, Zeyan Hu, Yong Luo*

Key Laboratory of Information Technology for AUVs, Institute of Acoustics, University of Chinese Academy of Sciences, North 4th Ring West Road No. 21, Haidian District, Beijing, People's Republic of China
✉ *E-mail: fengchaowill@hotmail.com*

Abstract: An improved discretisation method relative to the geometric dimensions of the rotor-bearing system in the calculation of its critical speeds using the transfer matrix method (TMM) is introduced to enhance the computation precision. This work is motivated by the noise analysis of the power system, wherein the noise source identification in a multiple source environment is challenging and hence the need for a higher degree of accuracy. This new discretisation method is derived according to the principles of the equivalence of mass properties with lumped mass and moment of inertia included. The efficiency of the proposed discretisation method is tested via both simulation studies and real noise data. The Riccati TMM is applied on the equivalent discrete models obtained from the proposed geometric dimension discretisation method (abbreviated to GDDM in this study) as well as the empirical discretisation formula, the comparison of which indicates that the analysis of the rotor-bearing assembly discretised appropriately enough under the GDDM is capable of providing solutions of critical speed and predictions of vibration modes and noise with better precision.

1 Introduction

The utilisation of high-speed permanent magnet (PM) motor in the power system is to be preferred in plenty of engineering applications [1, 2]. In the noise and vibration analysis of a rotating machinery, of great interest is the calculation of the rotor's critical speeds, because severe vibration or even damage could happen if the intended operating speed is close to or coincide with the critical speed [3]. The unexpected vibration could be detected by the spectrum of radiated noise acquired from experiments, which works in combination with the precise computation of critical speeds to achieve a comprehensive description of the structure-induced vibration characteristics of a power system.

The application of conventional approaches to compute the critical speeds, which is solving the differential equations of motion, is restricted due to its computational complexity. With the progress of high-performance computers, the finite element method (FEM) has been widely applied in that modelling and calculation of structures with complex shapes could be achieved through FEM. However, FEM has difficulties in the interpretation of some parameters with clear physical meanings and is usually time-consuming even for the high-performance computers [4]. The transfer matrix method (TMM) was first proposed by Myklestad and improved by Prohl [5, 6]. To improve the numerical stability of the Prohl TMM, the Riccati TMM was developed, where the formulation of the method was derived from the conversion of a two-point boundary value problem to an initial value problem [7]. The fundamental idea of TMM is to make the state variables on the cross-section transfer from one end of the rotor to the other according to the deformation compatibility condition. Thus, unlike FEM, the order of TM in TMM stays with the number of initial state variables and does not increase with the degree-of-freedom of the system. For this reason, the TMM is relatively easy to be programmed with less time and memory requirement during computing.

Many scholars have contributed to the analyses of rotor-bearing assemblies using the TMM [8–10], and the calculation precision of TMM is of great importance. Hsieh *et al.* [11] investigated the influence of extra forces on calculation precision and vibration mode prediction of a rotor-bearing system. Liu [12] adopted a recurrence perturbation formula based on the Riccati TMM instead of the conventional perturbation FEM for a more precise eigenvalue analysis of a rotor system with uncertain parameters.

To improve the calculation precision of the TMM, most of the researches focus on the assembly of the TM itself (e.g. [7]) and the optimisation of the solving algorithm (e.g. [13]). However, very little attention had been paid to the pre-process of the TMM which is the discretisation of the model, even for the general studies of this method [14, 15]. To apply the TMM, a typical elastic rotor-bearing system with continuous mass distribution first needs to be discretised into a certain number of segments along the axial direction. Horner and Pilkey [7] gave two conditions, based on which the structure should be segmented. They suggested that the length of each segment should be such that all of the terms comprising each element of the TM are approximately the same order of magnitude and a segmentation should occur where the state variables are desired. Nevertheless, these two conditions cannot give clear and precise directions for discretisation because they lack mathematical description. Huang and Han [16] adopted a condition with a definite mathematical formulation, which is

$$N \geq 1 + 5.34r \tag{1}$$

where N is the total number of lumped discs and r denotes the highest order of the natural frequency required.

However, (1) is only an empirical formula as clearly stated in [16], and the discrete model obtained from this empirical formula is still highly possible to give answers with the computing precision poorer than the value intended which is 1%. Since the discretisation of the rotor-bearing system is the premise of the following work of TMM, it is reasonable to assume that the structure characteristics related to the geometry dimensions of the

rotor should be taken into account as well as N and r [used in (1)] in the discretisation. Thus, it is the intent of this paper to provide valuable information on the optimisation of the pre-process in the application of TMM for computing the critical speed of a rotor-bearing assembly more precisely.

The remainder of this paper is organised as follows. In Section 2, the proposed quantitative discretisation method for rotors is strictly derived. In Section 3, necessary simulation studies are performed to evaluate the capability of the proposed geometric dimension discretisation method (GDDM) in improving the calculation accuracy of the Riccati TMM. Simulations of the discrete models obtained from the empirical formula are presented for performance comparison. Section 4 provides the further details and possible situations that may be encountered when using discrete model with larger number of elements under the GDDM. In Section 5, the proposed GDDM is applied on a rotor-bearing assembly from a PM motor to calculate its critical speed. Experimental data of the radiated noise of the same motor are recorded to support the calculated result given by the optimised discrete model. Finally, conclusions are drawn and a discussion of possible extensions is stated in Section 6.

2 Derivation of the GDDM

Usually, the rotor-bearing system is modelled by beam elements [17]. On this premise, the segments discretised from rotor-bearing system are divided into two different types: one is the elastic beam segment with only its diameter and length considered, while its mass and moment of inertia are lumped on each end of its own, wherein lies the other type of segment, the rigid disc. It should be noted that these discs are treated such as particles with no geometric dimensions taken into consideration. The rigid disc is addressed as point or station [18], and the beam segment as field.

2.1 Calculation of lumped mass

According to the invariant centroid theory [16], the mass of the rigid disc lumped on both ends of the jth beam segment is

$$\begin{cases} m_j^{\mathrm{R}} = \dfrac{\sum_{k=1}^{s} \mu_k l_k a_k}{l_j} \\ m_j^{\mathrm{L}} = \dfrac{\sum_{k=1}^{s} \mu_k l_k (l_j - a_k)}{l_j} \end{cases} \tag{2}$$

where the superscripts R and L refer to right and left, s is the number of sub-beams with different cross-section dimensions within the jth beam segment (see Fig. 1), l_j is the total length of the jth beam segment, l_k and μ_k ($k = 1, 2, \ldots, s$) are the length and the mass per unit length of the kth ($k = 1, 2, \ldots, s$) sub-beam, respectively, and a_k is the distance from the kth ($k = 1, 2, \ldots, s$) sub-beam's centroid to the left end cross-section of the jth beam segment.

2.2 Calculation of lumped moment of inertia

The moment of principal axes of inertia of the kth ($k = 1, 2, \ldots, s$) sub-beam with uniform cross-section dimension in the jth beam segment are given below [16]

$$\begin{cases} J_{pk} = j_{pk} l_k \\ J_{dk} = \displaystyle\int_{-(l_k/2)}^{l_k/2} \left[j_{dk}\, \mathrm{d}l + \mu_k\, \mathrm{d}l \cdot l^2 \right] = j_{dk} l_k + \frac{1}{12} \mu_k l_k^3 \end{cases} \tag{3}$$

where j_k ($k = 1, 2, \ldots, s$) is the moment of inertia per unit length, and the subscripts p and d refer to the polar and diameter moment of inertia, respectively.

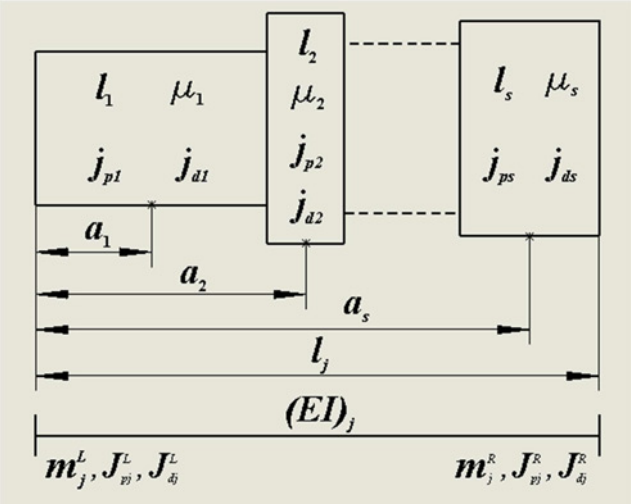

Fig. 1 *jth Beam segment with different cross-section dimensions*

Let $J_{pk}^{\mathrm{L}}, J_{pk}^{\mathrm{R}}, J_{dk}^{\mathrm{L}}$ and J_{dk}^{R} be the kth ($k = 1, 2, \ldots, s$) sub-beam's polar and diameter moment of inertia lumped on both ends of the jth beam segment. Then, the principles of the constant of moment of inertia can be described as

$$\begin{cases} J_{pk}^{\mathrm{L}} + J_{pk}^{\mathrm{R}} = J_{pk} = j_{pk} l_k \\ J_{dk}^{\mathrm{L}} + m_{jk}^{\mathrm{L}} a_k^2 + J_{dk}^{\mathrm{R}} + m_{jk}^{\mathrm{R}} \left(l_j - a_k \right)^2 = J_{dk} \end{cases} \tag{4}$$

in which

$$\begin{cases} m_{jk}^{\mathrm{R}} = \dfrac{\mu_k l_k a_k}{l_j} \\ m_{jk}^{\mathrm{L}} = \dfrac{\mu_k l_k \left(l_j - a_k \right)}{l_j} \end{cases} \tag{5}$$

Since the moment of inertia is inversely proportional to the square of distance [16], which is

$$\begin{cases} J_{pk}^{\mathrm{L}} a_k^2 = J_{pk}^{\mathrm{R}} \left(l_j - a_k \right)^2 \\ J_{dk}^{\mathrm{L}} a_k^2 = J_{dk}^{\mathrm{R}} \left(l_j - a_k \right)^2 \end{cases} \tag{6}$$

We combine (3)–(6), yielding

$$\begin{cases} J_{pk}^{\mathrm{R}} = \dfrac{a_k^2}{a_k^2 + \left(l_j - a_k \right)^2} j_{pk} l_k \\ J_{pk}^{\mathrm{L}} = \dfrac{\left(l_j - a_k \right)^2}{a_k^2 + \left(l_j - a_k \right)^2} j_{pk} l_k \\ J_{dk}^{\mathrm{R}} = \dfrac{a_k^2}{a_k^2 + \left(l_j - a_k \right)^2} \left[j_{dk} l_k + \dfrac{1}{12} \mu_k l_k^3 - \mu_k l_k a_k \left(l_j - a_k \right) \right] \\ J_{dk}^{\mathrm{L}} = \dfrac{\left(l_j - a_k \right)^2}{a_k^2 + \left(l_j - a_k \right)^2} \left[j_{dk} l_k + \dfrac{1}{12} \mu_k l_k^3 - \mu_k l_k a_k \left(l_j - a_k \right) \right] \end{cases} \tag{7}$$

IET Electr. Power Appl., 2017, Vol. 11, Iss. 7, pp. 1245–1253

Accordingly, the lumped moment of inertia on both ends of the jth beam segment can be expressed as

$$\begin{cases} J_{pj}^{\mathrm{R}} = \sum_{k=1}^{s} J_{pk}^{\mathrm{R}} \\ J_{pj}^{\mathrm{L}} = \sum_{k=1}^{s} J_{pk}^{\mathrm{L}} \\ J_{dj}^{\mathrm{R}} = \sum_{k=1}^{s} J_{dk}^{\mathrm{R}} \\ J_{dj}^{\mathrm{L}} = \sum_{k=1}^{s} J_{dk}^{\mathrm{L}} \end{cases} \tag{8}$$

2.3 Simplified formulation of the equivalent mass properties

For the reason of brevity and convenience, the jth beam segment is expected to be of uniform cross-section dimension, which gives

$$\begin{cases} s = 1 \\ l_k = l_j \\ a_k = l_j/2 \end{cases} \tag{9}$$

In this case, the equivalent mass and moment of inertia lumped on both ends of the jth beam segment can be re-expressed as

$$\begin{cases} m_j^{\mathrm{L}} = m_j^{\mathrm{R}} = \frac{1}{2}\mu_j l_j \\ J_{pj}^{\mathrm{L}} = J_{pj}^{\mathrm{R}} = \frac{1}{2} j_{pj} l_j \\ J_{dj}^{\mathrm{L}} = J_{dj}^{\mathrm{R}} = \frac{1}{2}\left(j_{dj} l_j - \frac{1}{6}\mu_j l_j^3 \right) \end{cases} \tag{10}$$

2.4 Geometric DDM

This paper has particular interest in the expression of the diameter moment of inertia J_{dj} [in (10)], because the definition of the moment of inertia [see Equation (11), [15], pp. 409–410] indicates that its value should be a positive value in the application of the TMM

$$J = \int r^2 \, \mathrm{d}m \tag{11}$$

Under this circumstance, a relation is established between the cross-section dimension of the jth beam segment and its length after discretisation. For solid shaft, we have

$$j_{dj} l_j - \frac{1}{6}\mu_j l_j^3 = \frac{1}{16}\mu_j D^2 l_j - \frac{1}{6}\mu_j l_j^3 > 0 \frac{l_j^2}{3} < \frac{D^2}{8} \tag{12}$$

Moreover, for hollow shaft

$$\begin{gathered} j_{dj} l_j - \frac{1}{6}\mu_j l_j^3 = \frac{1}{16}\mu_j \left(D^2 + d^2\right) l_j - \frac{1}{6}\mu_j l_j^3 > 0 \\ \frac{l_j^2}{3} < \frac{D^2 + d^2}{8} \end{gathered} \tag{13}$$

where D and d denote the outer and inner diameters of the jth beam's cross-section, respectively.

Here, expressions (12) and (13) are the quantitative GDDM suggested in this paper for the TMM.

3 Evaluation of GDDM in the Riccati method

In this section, the different discrete models of the same rotor-bearing assembly, whose first four orders of critical speed and the corresponding vibration mode curves are given for [19], are obtained from both the GDDM and empirical formula for comparison. The rotor shaft of the rotor-bearing system is 9.4 m long in the axial direction and the density of its material is 7550 kg/m^3, with 130 and 44 GPa as its elasticity and shear modulus, respectively. There are two identical flexible supports at both ends of it. The equivalent mass, static stiffness and oil film stiffness of the flexible supports are 1.764×10^4 kg, 3.92×10^9 N/m and 2.45×10^9 N/m, respectively.

The rotor shaft is numbered from 1 to 15 according to the change of cross-section, locations of attached components and its structural features, as shown in Fig. 2. Each of the shaft segment is of uniform cross-section dimension, and it will be discretised into some certain number of points and fields. Generally, the ith point and the ith field on its right compose the ith element (see Fig. 3).

Considering the rotor-bearing assembly is axially symmetric, a four-degrees-of-freedom rotor model is practicable here [15]. If we adopt y to represent the displacement in the vertical direction in Fig. 2, θ is the deflection of cross-section in the plane defined by the rotor axis and plumb line, M is the bending moment and Q is the shear force, the state vectors on the cross-section of the ith element can be written as

$$z_i = \begin{bmatrix} y & \theta & M & Q \end{bmatrix}_i^{\mathrm{T}} \tag{14}$$

3.1 Riccati method

The Riccati method has already been demonstrated and used to resolve real issues of rotor systems in plenty of literature related; hence, the detailed description of the method is not the primary interest of this paper and need not be repeated here, but the necessary information related to the form of TM and frequency governing equation will be described here for the sake of brevity.

Fig. 2 *Model of the rotor-bearing assembly to be analysed*

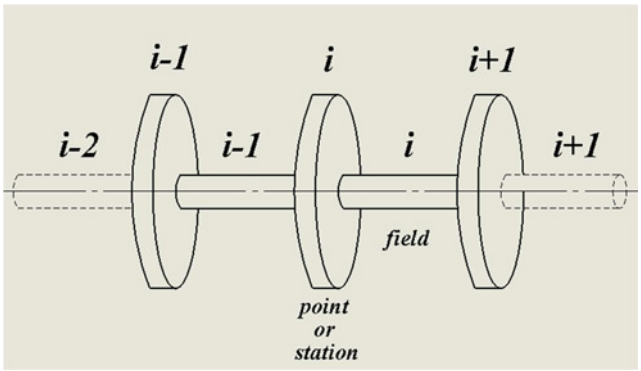

Fig. 3 *Discrete model with stations and fields*

Grounded on the principles of the Riccati TMM, the matrix of state variables $\boldsymbol{z}_i$ is reorganised as

$$\begin{Bmatrix} \boldsymbol{f} \\ \boldsymbol{e} \end{Bmatrix}_i$$

according to the condition of the state variables at the left-hand boundary of the system [7]. To be specific, $\{\boldsymbol{f}\}$ contains the $n/2$ (n is the total number of state variables) state variables that are homogeneous at the left-hand boundary (say their values are all zeros) and $\{\boldsymbol{e}\}$ contains the rest $n/2$ complementary state variables. The transfer of the state variables from point i to point $i+1$ can be described as follows:

$$\begin{Bmatrix} \boldsymbol{f} \\ \cdots \\ \boldsymbol{e} \end{Bmatrix}_{i+1} = \begin{bmatrix} \boldsymbol{u}_{11} & \vdots & \boldsymbol{u}_{12} \\ \cdots\cdots & \vdots & \cdots\cdots \\ \boldsymbol{u}_{21} & \vdots & \boldsymbol{u}_{22} \end{bmatrix}_i \begin{Bmatrix} \boldsymbol{f} \\ \cdots \\ \boldsymbol{e} \end{Bmatrix}_i \tag{15}$$

where

$$\begin{cases} [\boldsymbol{u}_{11}]_i = \begin{bmatrix} 1 & l \\ 0 & 1 \end{bmatrix}_i \\ [\boldsymbol{u}_{12}]_i = \begin{bmatrix} l(\omega^2 m - k) & \left(J_\mathrm{p} - J_\mathrm{d}\dfrac{\Omega}{\omega}\right)\omega^2 \\ \omega^2 m - k & 0 \end{bmatrix}_i \\ [\boldsymbol{u}_{21}]_i = \begin{bmatrix} \dfrac{l^2}{2EI} & \dfrac{l^3}{6EI}(1-\gamma) \\ \dfrac{l}{EI} & \dfrac{l^2}{2EI} \end{bmatrix}_i \\ [\boldsymbol{u}_{22}]_i = \begin{bmatrix} 1 + \dfrac{l^3}{6EI}(1-\gamma)(\omega^2 m - k) & l + \dfrac{l^2}{2EI}\left(J_\mathrm{p} - J_\mathrm{d}\dfrac{\Omega}{\omega}\right)\omega^2 \\ \dfrac{l^2}{2EI}(\omega^2 m - k) & 1 + \dfrac{l}{EI}\left(J_\mathrm{p} - J_\mathrm{d}\dfrac{\Omega}{\omega}\right)\omega^2 \end{bmatrix}_i \end{cases} \tag{16}$$

In (16), EI is the bending stiffness, k is the stiffness of the elastic support on the ith point (taken as zero if there is not any), ω is the whirl speed, Ω is the spin speed (we take $\Omega = \omega$ in this paper) and γ is the shear influence coefficient of the ith field cross-section, which is defined as

$$\gamma = \left(\frac{6EI}{aGAl^2}\right)_i \tag{17}$$

where A denotes the cross-section area, G is the shear modulus and a is the factor related to the cross-section shape (for the hollow circular section, a is taken as 0.667; for the solid circular section, a is taken as 0.886).

Then the Riccati transformation is introduced [7]

$$\{\boldsymbol{f}\}_i = [\boldsymbol{s}]_i\{\boldsymbol{e}\}_i \tag{18}$$

where the $(n/2) \times (n/2)$ matrix $[\boldsymbol{s}]_i$ is the Riccati TM. By combining (15) and (18), the recursion formula of the Riccati TM is obtained

$$[\boldsymbol{s}]_{i+1} = [\boldsymbol{u}_{11}\boldsymbol{s} + \boldsymbol{u}_{12}]_i[\boldsymbol{u}_{21}\boldsymbol{s} + \boldsymbol{u}_{22}]_i^{-1} \tag{19}$$

Considering the deformation compatibility requirements of the flexible constraints, the frequency governing equation of the Riccati TMM in this case can be expressed as

$$|s|_{N+1} = \begin{vmatrix} s_{11} & s_{12} \\ s_{21} & s_{22} \end{vmatrix}_{N+1} = 0 \tag{20}$$

where $|s|$ denotes the determinant of the square matrix $[\boldsymbol{s}]$.

It is worth noting that the solving algorithm applied in this paper is modified by substituting (20) with (21), which can eliminate the singular points in solving the frequency equation, hence the improvement of numerical stability [20]

$$D_1(\omega^2) = |S|_{N+1}\prod_{i=1}^{N}\mathrm{Sign}\left(\left|[u_{21}s + u_{22}]_i\right|\right) = 0 \tag{21}$$

3.2 Simulation satisfying the proposed GDDM

Here, the rotor-bearing system is discretised into 29 elements premised on the proposed GDDM. The details of this discretisation are listed in Table 1. It should be noted that 29 is the minimum number of elements to satisfy the proposed GDDM for this rotor.

Then, the modified Riccati method is performed on this discrete model and the first four orders of critical speed are computed as well as the corresponding vibration modes (as illustrated in Fig. 4). The comparison between the calculated speeds and the reference values is shown in Table 2 and the relative percentage error is obtained. It can be seen that the relative errors are all <1%, which are also reflected in the differences between the computed and reference mode curves in Fig. 4. In general, the vibration mode curves calculated from the discrete model under the GDDM are in conformity with the trend of the curves for reference despite the small differences in the amplitude.

3.3 Simulations only satisfying the empirical formula

In this section, the rotor-bearing assembly is discretised in manners that satisfy the empirical formula only, which indicates that 22 elements with 23 points will be enough for the computation of first four orders of critical speed.

3.3.1 Discretisation manner 1: In this manner, the 2nd, 5th and 11th shaft segments will all be discretised into two elements with different lengths. To be specific, the 2nd into 0.4 and 0.105 m in length, the 5th and 11th both into 0.48 and 0.1 m. Besides, the 4th shaft segment will be divided into four equal elements, and the 7th as well as the 9th into three. The 14th and 15th will be bisected, while the 8th will remain in one piece. The rest shaft segments will be the same as stated in Table 1. As a result, the rotor-bearing

Table 1 Details of the discrete model with 29 elements under GDDM

Shaft segment			Element	
Segment number	Diameter, m	Length, m	Number of elements after discretisation	Length, m
1	0.47	0.275	1	0.2750
2	0.57	0.505	2	0.2525
3	0.59	0.365	2	0.1825
4	0.71	0.475	2	0.2375
5	0.72	0.580	2	0.2900
6	1.01	0.100	1	0.1000
7	1.03	0.650	2	0.3250
8	1.02	3.900	7	0.5517
9	1.03	0.650	2	0.3250
10	1.01	0.100	1	0.1000
11	0.71	0.580	2	0.2900
12	0.69	0.275	1	0.2750
13	0.58	0.365	2	0.1825
14	0.55	0.295	1	0.2950
15	0.47	0.285	1	0.2850

IET Electr. Power Appl., 2017, Vol. 11, Iss. 7, pp. 1245–1253

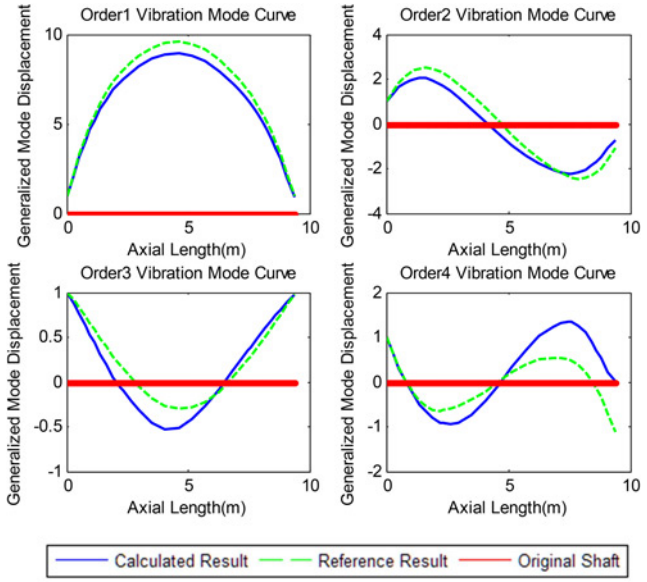

Fig. 4 *Vibration mode curves corresponding to the discrete models with 29 elements under GDDM*

Table 2 First four orders of the critical angular speed calculated from the discrete model with 29 elements created under GDDM

Order of critical speed	Reference value, rad/s	Calculated value, rad/s	Relative error, %
1	93.5719	94.2707	0.747
2	287.5432	289.5848	0.710
3	459.9533	460.6963	0.162
4	498.8326	503.7099	0.978

assembly is also modelled by 29 elements, but some of the elements in the 2nd, 5th, 8th and 11th shaft segments do not satisfy the proposed GDDM. The calculation results are shown in Table 3.

The relative errors calculated from the discrete model only satisfying the empirical formula are much larger than those in Section 3.2 (as shown in Table 2), even though they have the same number of elements. This is because each of the elements which do not satisfy the GDDM makes the value of its diameter moment of inertia negative. In the TM of the state variables, there is a term with reference to the polar and diameter moment of inertia [see $[\boldsymbol{u}_{12}]_i$ and $[\boldsymbol{u}_{22}]_i$ in (16)], which is $J_\mathrm{p} - J_\mathrm{d}$. For solid shaft, we have

$$J_\mathrm{p} - J_\mathrm{d} = \frac{1}{16}\mu_j D^2 l_j + \frac{1}{6}\mu_j l_j^3 \tag{22}$$

and for hollow shaft

$$J_\mathrm{p} - J_\mathrm{d} = \frac{1}{16}\mu_j (D^2 + d^2) l_j + \frac{1}{6}\mu_j l_j^3 \tag{23}$$

Since none of the values of μ_j and l_j are negative, we know from (22) and (23) that the value of the term $J_\mathrm{p} - J_\mathrm{d}$ is always positive, which indicates that $J_\mathrm{p} > J_\mathrm{d}$. In the situation where we have a positive value of J_d through the GDDM, the value of term $J_\mathrm{p} - J_\mathrm{d}$ is smaller than J_p, whereas it can be larger than J_p in the situation where we have negative value of J_d such as the discretisation manner 1 in this section. Solving the frequency governing [see (21)] requires computing the cumulative product of each discrete element's TM. A large value of matrix element is undesirable, because it could make the value of the matrix element in the final matrix $[\boldsymbol{S}]_{N+1}$ considerably large, which would result in the undesirable subtraction of two large numbers and poor accuracy, especially when these two numbers are close to each other (the reason is provided in details via Appendix 1). The corresponding vibration mode curves are obtained from the calculated critical speeds. Since the computed critical speeds diverge greatly from the reference values, the corresponding mode curves will not be in conformity with the reference curves. Fig. 5*a* depicts the great difference between the calculated and reference vibration mode curves in this section.

Table 3 First four orders of the critical angular speed calculated from the discrete model with 29 elements, some of which disobey the proposed GDDM, however, satisfy the empirical formula

Order of critical speed	Reference value, rad/s	Calculated value, rad/s	Relative error, %
1	93.5719	100.8705	7.800
2	287.5432	261.1742	9.170
3	459.9533	468.2168	1.797
4	498.8326	485.0791	2.757

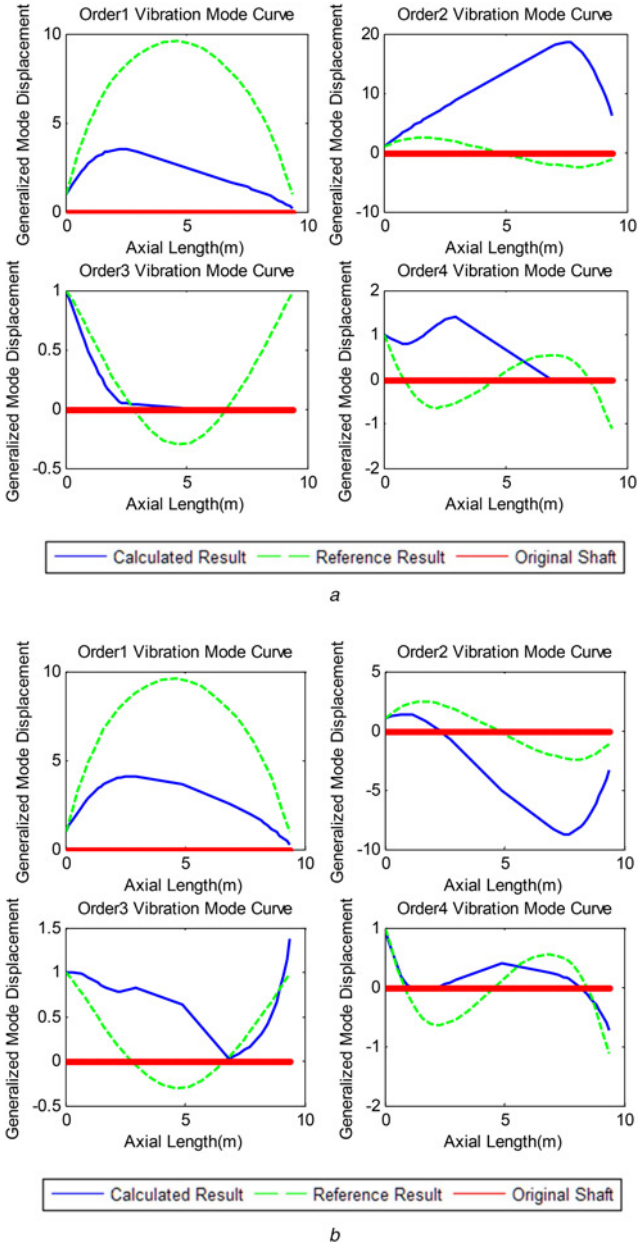

Fig. 5 *Vibration mode curves of the discrete model under empirical formula*

a Vibration modes curves corresponding to discretisation manner 1
b Vibration modes curves corresponding to discretisation manner 2

3.3.2 Discretisation manner 2: The discrete model of the rotor-bearing assembly used in this manner is basically the same as that in Section 3.3.1, except for the discretisation of the 1st, 8th and 12th segments. These three segments are all bisected in this section, which gives 32 elements and 33 points, the most number of elements by now. Similarly, the proposed GDDM are not satisfied here, while the demand for elements in the empirical formula is met. The first four orders of critical speed calculated here are summarised in Table 4.

Table 4 gives better precision of the critical speed than Table 3, in that the TMM adopts a discrete model with all its constituent elements concatenated in the axial direction to simulate a rotor-bearing system, the mass of which is continuously distributed in fact, the equivalence tends to be more effective when more elements are applied. It is important to note that this comparison is made in the circumstance that the equivalent models are discretised under the same condition, which is the empirical formula as shown in (1). However, in comparison of the accuracy from Tables 2 and 4, using the empirical condition to create a discrete model with more elements seems no longer to be a fully dominating method, for the same reason discussed in Section 3.3.1. Fig. 5*b* presents the vibration mode curves corresponding to the calculated results in Table 4. They appear to be a better approximation to the reference result compared with Fig. 5*a*. Since the curves presented in Fig. 5*b* are still calculated from the critical speeds with poor precision, their approximation to the reference result remains inferior to that in Section 3.2 under the GDDM.

4 Increasing the number of elements under the GDDM

From the expression of the GDDM [see (12) and (13)], we note that for a system with determinate cross-section dimensions, the more elements created in its discrete model, the smaller the value of l_j will be, hence the easier it will be to satisfy (12) or (13). In this case, Section 4 will give a further discussion of the situation where the number of elements is increased under the GDDM.

4.1 Discrete model with 49 elements under the GDDM

Table 5 displays the details of the discretisation for the model adopted in this section. This equivalent model has 49 elements and 50 points; moreover, all of these elements satisfy the GDDM.

We apply the modified Riccati method on the above model. The calculated results are shown in Table 6 and the corresponding vibration mode curves in Fig. 6.

From Table 6, we can see that all of the relative error values fall below 0.1%, which is vastly superior to the other methods mentioned above. Besides, the calculated vibration mode curves presented in Fig. 6 are in good conformity with the reference result. It appears that increasing the number of elements under the GDDM could further the improvement of the computing precision of the Riccati TMM. However, further increase of the number of elements is not suggested here because it would bring an $[\boldsymbol{s}]_{N+1}$ with considerably large values of the matrix elements, hence the decline in the calculation precision (the reason is provided in details via Appendix 1, and a numerical result is given in Appendix 2). It should be noted that the reason of the decline in the calculation precision here is different from that in Section 3.3. In this section, it is the number of times doing the multiplication in computing the cumulative product of each discrete element's TM that leads to the large values of matrix element in $[\boldsymbol{s}]_{N+1}$, whereas the major cause is the increment value of matrix element in some discrete element's TM. In Section 3.3, both of these two problems could be avoided using the GDDM.

Table 4 First four orders of the critical angular speed calculated from the discrete model with 32 elements, some of which disobey the proposed GDDM, however, satisfy the empirical condition

Order of critical speed	Reference value, rad/s	Calculated value, rad/s	Relative error, %
1	93.5719	95.1175	1.652
2	287.5432	291.2209	1.279
3	459.9533	453.9564	1.304
4	498.8326	505.2376	1.284

Table 5 Details of the discrete model with 49 elements under GDDM

Shaft segment			Element	
Segment number	Diameter, m	Length, m	Number of elements after discretisation	Length, m
1	0.47	0.275	1	0.2750
2	0.57	0.505	3	0.1683
3	0.59	0.365	2	0.1825
4	0.71	0.475	3	0.1583
5	0.72	0.580	3	0.1933
6	1.01	0.100	1	0.1000
7	1.03	0.650	3	0.2167
8	1.02	3.900	19	0.2053
9	1.03	0.650	3	0.2167
10	1.01	0.100	1	0.1000
11	0.71	0.580	3	0.1933
12	0.69	0.275	1	0.2750
13	0.58	0.365	2	0.1825
14	0.55	0.295	2	0.1475
15	0.47	0.285	2	0.1425

Table 6 First four orders of the critical angular speed calculated from the discrete model with 49 elements created under GDDM

Order of critical speed	Reference value, rad/s	Calculated value, rad/s	Relative error, %
1	93.5719	93.5831	0.012
2	287.5432	287.7405	0.069
3	459.9533	460.0743	0.026
4	498.8326	498.9880	0.031

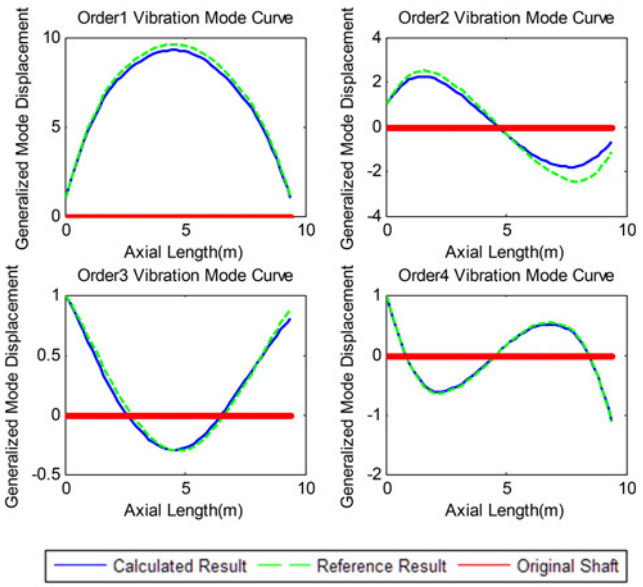

Fig. 6 *Vibration mode curves corresponding to the discrete models with 49 elements under GDDM*

5 Radiated noise data analysis

In this section, the radiated noise from a PM motor (see Fig. 7*a*) is recorded for further analysis.

IET Electr. Power Appl., 2017, Vol. 11, Iss. 7, pp. 1245–1253

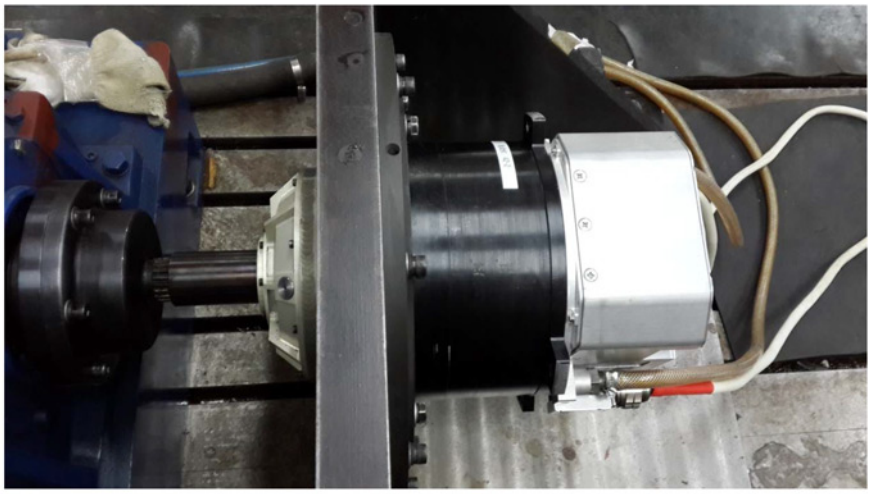

a

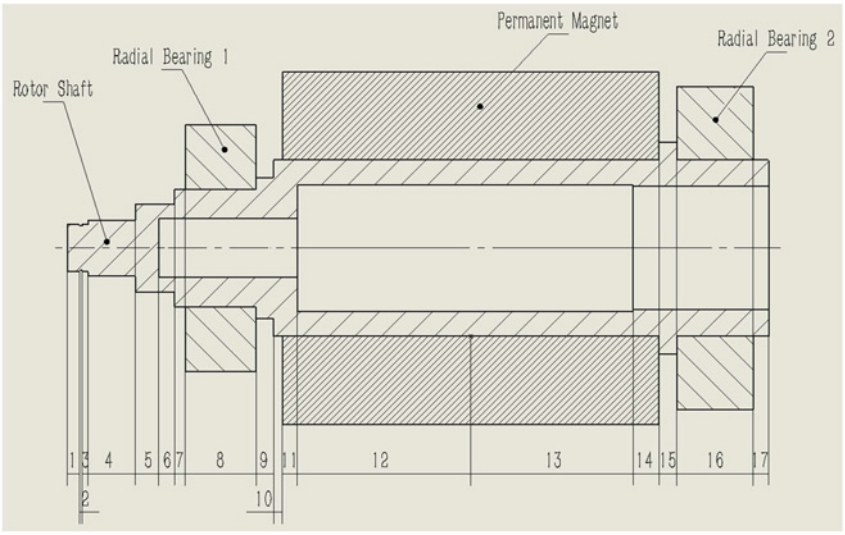

b

Fig. 7 *PM motor and the rotor shaft assembly*

a Arrangement of radiated noise measurement of the PM motor
b Motor's rotor shaft assembly

The schematic representation of the motor's rotor shaft assembly is illustrated in Fig. 7*b*, and material properties of its main components are listed in Table 7.

In the radiated noise measurement of the PM motor, four different operating conditions are examined, the rotational speeds of which are 4300, 6400, 8000 and 11,000 revolutions per minute. The corresponding frequencies of these four operating conditions are 72, 107, 133 and 183 Hz. Fig. 8 presents the radiated noise spectrum under the four operating conditions mentioned above. It can be seen that the radiated noise energy of the operating condition of 11,000 r/min is generally at a higher level than the other operating conditions. For the operating condition of 11,000 r/min, the amplitude of radiated noise energy at frequency

Table 7 Material properties of the main components of the motor's rotor shaft assembly

Component	Material	Elasticity modulus, GPa	Density, kg/m^3	Poisson ratio
shaft	30CrMnSiA	172	7850	0.28
PM	Sm2Co17	100	8400	0.30
radial bearing	Cr–Ni alloy steel	207	7810	0.29

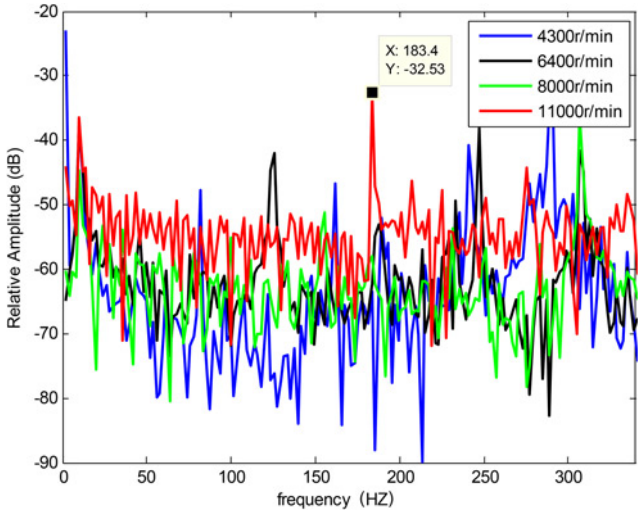

Fig. 8 *Radiated noise spectrum under different operating conditions*

Table 8 First order of the critical speed calculated from two different discretisation methods

	GDDM	Empirical formula
critical rotational speed, revolutions/min	11,100	11,760
corresponding angular velocity, rad/s	1162	1232
corresponding frequency, Hz	185	196

183 Hz corresponding to this rotational speed is much greater than the other locations. From these two evidences, it is reasonable to conclude that the rotational speed 11,000 r/min is one of the critical speeds of the rotor system in this PM motor [16].

The first order of critical speed calculated from the discrete model obtained from the proposed GDDM and the empirical formula is shown in Table 8, which complies well with the experimental analysis above that excessive vibration and higher power of radiated noise is to be expected near the rotational speed of 11,000 r/min.

Comparing the results calculated from the two different discretisation methods, the discrete model obtained from the proposed GDDM gives a relative error of 0.87% to the measured value 11,000 r/min, whereas the relative error of the discrete model obtained from the empirical formula is 6.9%. Thus, the superior performance of the proposed GDDM over the empirical formula is validated through the radiated noise data analysis.

6 Conclusion and discussion

This paper focuses mainly on the pre-processing of the TMM used in the critical speed analysis of the rotor-bearing assembly, which is the discretisation of the system model. A new discretisation method, derived according to the principles of mass equivalence, is introduced, examined and proved capable of giving answers with better precision than the empirical formula by the simulations of a certain rotor-bearing system in the Riccati TMM. The empirical formula is more likely to generate J_d with negative value, hence the poor approximation of the rotor-bearing system.

Furthermore, better precision could be achieved by appropriately increasing the element number under the GDDM. However, excess number of elements cannot improve the accuracy of computation, but only add to the redundant workload. It is suggested in this paper that the optimised lower limit of the number of elements, given by the GDDM, would be appropriately enough for the discretisation of a rotor-bearing assembly in the engineering applications. In addition, the superior performance of the proposed GDDM over the empirical formula is validated through radiated noise data analysis.

Of great interest is the future work on the solution of the upper limit of the number of elements. It can be concluded that the poor precision results from the calculation of the cumulative product of TM and the number of times doing the multiplication is closely related to the number of elements. Thus, a relationship between the number of elements and the calculation accuracy requirement could be obtained. However, the complex structure of the rotor shaft complicates this process. The correlative study will be reported in future publication.

7 Acknowledgment

This work was supported by the National Natural Science Foundation of China under grant 61471352, 61302169, 61531018 and 61372181.

8 References

1 Boglietti, A., Gerada, C., Cavagnino, A.: 'High speed electrical machines and drives', *IEEE Trans. Ind. Electron.*, 2014, **61**, (6), pp. 2943–2945
2 Gerada, D., Mebarki, A., Brown, N.L., *et al.*: 'High-speed electrical machines: technologies, trends, and developments', *IEEE Trans. Ind. Electron.*, 2014, **61**, (6), pp. 2946–2959
3 Tenconi, A., Vaschetto, S., Vigliani, A.: 'Electrical machines for high-speed applications: design considerations and tradeoffs', *IEEE Trans. Ind. Electron.*, 2014, **61**, (6), pp. 3022–3029
4 Yuan, H.: 'Matrix analysis method for complex rotor system' (Liaoning Science and Technology Press, 2014, 1st edn.), pp. 1–19
5 Myklestad, N.O.: 'A new method of calculating natural modes of uncoupled bending vibration of airplane wings and other types of beams', *J. Aeronaut. Sci.*, 1944, **11**, pp. 153–162
6 Prohl, M.A.: 'A general method of calculating critical speeds of flexible rotors', *J. Appl. Mech.*, 1945, **12**, (3), pp. 142–148
7 Horner, G.C., Pilkey, W.D.: 'The Riccati transfer matrix method', *ASME J. Mech. Des.*, 1978, **100**, (2), pp. 297–302
8 Lund, J.W., Wang, Z.: 'Application of the Riccati method to rotor dynamic analysis of long shafts on a flexible foundation', *J. Vib. Acoust.*, 1986, **108**, (2), pp. 177–181
9 Friswell, M.I., Gravey, S.D., Penny, J.E.T., *et al.*: 'Computing critical speeds for rotating machines with speed dependent bearing properties', *J. Sound Vib.*, 1998, **213**, (1), pp. 139–158
10 Bashir Asdaque, P.M.G., Behera, R.K.: 'Vibration analysis of hollow tapered shaft rotor', *Adv. Acoust. Vib.*, **2014**, (6), pp. 1–14
11 Hsieh, S.C., Chen, J.H., Lee, A.C.: 'A modified transfer matrix method for the coupling lateral and torsional vibrations of symmetric rotor-bearing systems', *J. Sound Vib.*, 2006, **289**, (1/2), pp. 294–333
12 Liu, B.G.: 'Eigenvalue problems of rotor system with uncertain parameters', *J. Mech. Sci. Technol.*, 2012, **26**, (1), pp. 1–10
13 Lund, J.W.: 'Stability and damped critical speed of a flexible rotor in fluid-film bearings', *ASME Trans. J. Eng. Ind.*, 1974, **96**, (2), pp. 509–517
14 Pestel, E.C., Leckie, F.A.: 'Matrix methods in elastomechanics' (McGraw-Hill, New York, 1963, 1st edn.)
15 Ishida, Y., Yamamoto, T.: 'Linear and nonlinear rotordynamics: a modern treatment with applications' (Wiley-VCH, Weinheim, 2012, 2nd edn.), pp. 351–372
16 Huang, Z.Y., Han, B.C.: 'Effective approach for calculating critical speeds of high speed permanent magnet motor rotor shaft assemblies', *IET Electr. Power Appl.*, 2015, **9**, (9), pp. 628–633
17 Ruhl, R.L., Booker, J.F.: 'A finite element model for distributed parameter turborotor systems', *ASME Trans. J. Eng. Ind.*, 1972, **94**, (1), pp. 126–132
18 Nelson, H.D., McVaugh, J.M.: 'The dynamics of rotor-bearing systems using finite elements', *ASME Trans. J. Eng. Ind.*, 1976, **98**, (2), pp. 593–600
19 Yuan, H.: 'Matrix analysis method for complex rotor system' (Liaoning Science and Technology Press, Shenyang, 2014, 1st edn.), pp. 26–27
20 Wang, Z.: 'The singularity of the Riccati transfer matrix method and a method for its being eliminated', *J. Vib. Shock*, **1987**, (2), pp. 74–78

9 Appendix

9.1 Appendix 1

Let $\bar{x}$ be the approximation of true value x, then the absolute error of $\bar{x}$ is defined as

$$e_x^- = x - \bar{x} \tag{24}$$

Another concept used to measure the extent of approximation is the relative error which is

$$r_x^- = \frac{e_x^-}{\bar{x}} = \frac{x - \bar{x}}{\bar{x}} \tag{25}$$

Since the difference in value between x and $\bar{x}$ is relatively small, we use the differential form of x to denote the absolute error e_x^-

$$e_x^- = x - \bar{x} = \mathrm{d}x \tag{26}$$

We continue by defining z as a function of x and y [see (27)]. This function, meanwhile, is regarded as differentiable with respect to x and y

$$z = f(x,\ y) \tag{27}$$

If we employ the approximations of x and y, which are $\bar{x}$ and $\bar{y}$, to calculate the value of $f(x,\ y)$, we have

$$\bar{z} = f(\bar{x},\ \bar{y}) \tag{28}$$

Table 9 First four orders of the critical angular speed calculated from the discrete model with 98 elements created under GDDM

Order of critical speed	Reference value, rad/s	Calculated value, rad/s	Relative error, %
1	93.5719	95.4074	1.962
2	287.5432	291.8599	1.501
3	459.9533	467.9162	1.731
4	498.8326	498.3659	0.094

Then the absolute error of $\bar{z}$ can be described as

$$e_z^- = z - \bar{z} = f(x,\ y) - f(\bar{x},\ \bar{y}) \tag{29}$$

According to (26), e_z^- could also be written as

$$e_z^- = \mathrm{d}z = \mathrm{d}f(x,\ y) = \frac{\partial f}{\partial x}\cdot \mathrm{d}x + \frac{\partial f}{\partial y}\cdot \mathrm{d}y \tag{30}$$

We can substitute dx and dy in (30) with e_x^- and e_y^-, respectively, yielding

$$e_z^- = \frac{\partial f}{\partial x}\cdot e_x^- + \frac{\partial f}{\partial y}\cdot e_y^- \tag{31}$$

Thus, the relative error of $\bar{z}$ can be expressed as

$$r_z^- = \frac{e_z^-}{\bar{z}} = \frac{\partial f}{\partial x}\cdot\frac{\bar{x}}{\bar{z}}\cdot\frac{e_x^-}{\bar{x}} + \frac{\partial f}{\partial y}\cdot\frac{\bar{y}}{\bar{z}}\cdot\frac{e_y^-}{\bar{y}} \tag{32}$$

The specific form of the function $f(x,\ y)$ we are interested in is

$$z = f(x,\ y) = x - y \tag{33}$$

By substituting (33) into (32), we arrive at the result

$$r_z^- = \frac{\bar{x}}{\bar{x}-\bar{y}}\cdot r_x^- - \frac{\bar{y}}{\bar{x}-\bar{y}}\cdot r_y^- \tag{34}$$

In addition, we note that for values of $\bar{y} = K\bar{x}$ (K is a real constant), (34) can be simplified as

$$r_z^- = \frac{r_x^- - K\cdot r_y^-}{1-K} \tag{35}$$

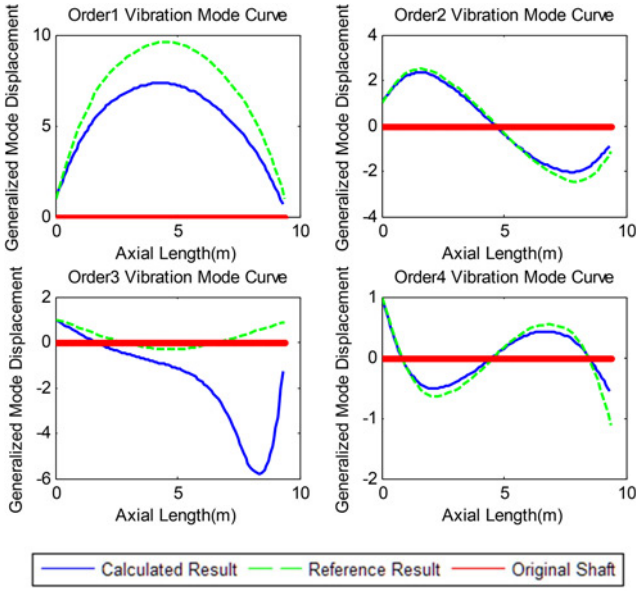

Fig. 9 *Vibration mode curves corresponding to the discrete models with 98 elements under GDDM*

Since the values of $\bar{x}$ and $\bar{y}$ are very large, they could be quite close quantitatively in the computing processing, which makes K approach the value 1, and hence

$$\begin{cases} \lim\limits_{K\to 1^-} r_z^- = \begin{cases} -\infty,\ r_x^- < r_y^- \\ \infty,\ r_x^- > r_y^- \end{cases} \\ \lim\limits_{K\to 1^+} r_z^- = \begin{cases} \infty,\ r_x^- < r_y^- \\ -\infty,\ r_x^- > r_y^- \end{cases} \end{cases} \tag{36}$$

Equation (36) indicates that the relative error in computation could be so large that numerical instability might occur in the process of calculating the subtraction of two large numbers.

9.2 Appendix 2: discrete model with 98 elements under the GDDM

See Table 9 and Fig. 9.